



## Toward an assessment of cleaning treatments onto nineteenth–twentieth-century photographs by using a multi-analytic approach

M. Romani<sup>1</sup> , L. Pronti<sup>1,a</sup> , C. Ruberto<sup>3,4</sup> , L. Severini<sup>2</sup> , C. Mazzuca<sup>2</sup> , G. Viviani<sup>1</sup>, A. Mazzinghi<sup>3,4</sup> , M. Chiari<sup>3</sup> , L. Castelli<sup>3</sup> , F. Taccetti<sup>3</sup> , A. Damiani<sup>5</sup>, C. Gorga<sup>6</sup>, M. Angelucci<sup>1</sup> , M. Cestelli-Guidi<sup>1</sup>

<sup>1</sup> INFN-Laboratori Nazionali di Frascati, Via Enrico Fermi 54, 00044 Frascati (RM), Italy

<sup>2</sup> Department of Chemical Science and Technologies, University of Rome “Tor Vergata”, Via della Ricerca Scientifica 1, 00133 Rome, Italy

<sup>3</sup> INFN-Sezione di Firenze, Via Bruno Rossi 1, 50019 Sesto Fiorentino (FI), Italy

<sup>4</sup> Dipartimento di Fisica e Astronomia, Università degli Studi di Firenze, Via G. Sansone 1, 50019 Sesto Fiorentino (FI), Italy

<sup>5</sup> Guest Student at INFN-Laboratori Nazionali di Frascati, Via Enrico Fermi 54, 00044 Frascati (RM), Italy

<sup>6</sup> Freelance Restorer, Rome (RM), Italy

Received: 7 March 2022 / Accepted: 13 June 2022

© The Author(s), under exclusive licence to Società Italiana di Fisica and Springer-Verlag GmbH Germany, part of Springer Nature 2022

**Abstract** The application of cleaning treatments for the restoration of nineteenth–twentieth-century photographs represents an innovative and still little explored aspect. In this work, in order to remove the degradation products, two cleaning methods were used for two different photographic techniques: poly(vinyl alcohol)-based hydrogels were applied to clean an albumen-based print, while calcium chlorine was used to remove the silver mirroring effect on a gelatin silver print. The constituent materials and conservation state of the analyzed photographs were characterized using a multi-analytical approach: imaging analyses (UV–VIS–NIR), attenuated total reflection (ATR) Fourier transform infrared spectroscopy (FT-IR) spectroscopy, macro-X-ray fluorescence scanning (MA-XRF) spectroscopy, pH analyses and particle-induced X-ray emission (PIXE) were applied before and after the cleaning treatments. The two treatments have permitted of the recovery the degraded parts of the two photos, especially in the first study case. For the silver mirroring effect, further treatments will be required to obtain a complete removal of the effect.

### 1 Introduction

In the field of Cultural Heritage, the restoration of photographs is a relatively recent branch. The most important operation of conservation is certainly the surface cleaning, but the choice of the suitable treatments is closely related to the constituent materials of the object. The photographic material developed during the nineteenth–twentieth century have been often realized by mixture of inorganic and organic materials. In the literature several studies are available regarding the characterization of the photograph's constituent materials and their conservation state [1–3]. However, the evaluations of surface cleaning treatments are still little explored. Unfortunately, this material cannot be treated with water-based products, unlike most artworks on paper, and therefore, restorers do not have many possibilities for conservation. The complexity of the examined materials shows the need of a multi-analytical approach to have a complete characterization [4, 5]. Another aspect to take in consideration regards the characterization of their degradation products. Albumen prints have very thin paper supports and usually are attached to a wood pulp cardboard support, easily degradable: they suffer from thermo-hygrometric variations and atmospheric factors that cause cracking, yellowing and discoloration of the emulsion [6]. Moreover, prints obtained with this type of photographic technique, which involves organic materials, are also affected by biodegradation damages, and several studies which describe how to recognize the different microorganisms are available [7]. Similar problems have also been observed for the gelatin-silver-based print [8]. This last type of prints is often DOP (developing-out paper) instead of POP (printing-out paper), like albumen prints, and their most common damage is a superficial degradation known as *silver mirroring*: this appears as a metallic reflected patina with a blue shade, as a mirror [9, 10]. It is a superficial layer of  $\text{Ag}^\circ$  or  $\text{Ag}_2\text{S}$ , due to interaction with the atmospheric factors and a wrong fixing procedure during the development of the photograph where the grains of metallic silver, which are formed during the development of the image, have dimensions of the order of microns and have a complex dendritic shape [9, 10].

In this work, a multi-analytical approach was used to characterize the constituent materials and their respective degradation products of an albumen print and a gelatin silver print that are representative of two different techniques used in the past to realize photographs [5, 11–13]. These methodologies are also useful to find possible solutions to the challenge related to surface cleaning treatments.

<sup>a</sup> e-mail: [lucilla.pronti@lnf.infn.it](mailto:lucilla.pronti@lnf.infn.it) (corresponding author)

At first, images in the UV-VIS-NIR were recorded in order to determine the presence of degradation products or biological attacks on the photographic surfaces (UV) [14, 15] and to study the spectral behavior of the constituent materials in the Near Infrared (NIR) range [16]. After this preliminary investigation, Fourier transform infrared spectroscopy (FT-IR) in ATR (attenuated total reflectance) mode was used to characterize the supports, the emulsions and the fillers [17–19]. Scanning electron microscopy with energy-dispersive X-ray spectroscopy (SEM-EDX), macro-X-ray fluorescence (MA-XRF) and particle-induced X-ray emission (PIXE) were performed in order to identify the elemental composition, to reveal the presence of elements that could derive from a wrong removal of fixatives during the manufacture process and to obtain information about the stratigraphy of the photographs [1, 20, 21]. The most appropriate cleaning treatments were chosen after the photographs characterization in order to remove the degradation products and to recover the original features [22, 23]. Poly(vinyl alcohol)-based hydrogels have been used for the albumen based photograph, while the gelatin silver print was subjected to a dry cleaning treatment, with the aim of removing the silver mirroring layer. It should be mentioned that the treatment of the silver mirror is controversial: in literature several studies do not recommend its removal as it is considered a natural modification of the original photo and not a degradation of it [24]. In this work we decide to consider it as a degradation product in order to recover the image. The analytical protocol used for the characterization of the constituent materials was adopted also to evaluate the efficacy of the cleaning processes with the addition of pH analyses for the albumen-based photograph.

## 2 Materials and methods

### 2.1 Materials samples

The photographs studied in this work are part of a private collection.

- **Sample 1 (S1):** The S1 (Fig. 1A) has been identified, through a visual analysis, as an albumin photograph [25]. The picture represents Trafalgar Square in London; no certain information about the date of its realization is available.
- **Sample 2 (S2):** The S2 (Fig. 1B) has been identified as a silver photograph, specifically a positive, because it does not present the inverted chiaroscuro. It is characterized by a surface deterioration (silver mirroring), typical degradation of gelatin silver prints DOP that appears as a “mirror” patina on the surface of the photograph [10]. This photo is dated in 1912.

### 2.2 Experimental setups

#### 2.2.1 Imaging analyses (UV-VIS-NIR)

UV fluorescence (UVF) imaging were realized by using a modified Reflex Camera Nikon D7000-NIR, with a silicon sensor and a spectral range between 370–1100 nm, with a resolution of 16.2 Megapixel. For the illumination, two UV lamps at 365 nm were used. Infrared reflectography (IRR) was performed by using the same Reflex Camera Nikon D700-NIR coupled with a 250 Watt halogen lamp.

#### 2.2.2 FT-IR analyses in ATR mode

FT-IR analyses in ATR mode were realized by using a Tensor II spectrometer (Bruker Optics, Germany), equipped with a diamond reflection element (Platinum ATR accessory) and a DTGS detector. The measurements were collected in the range 4000–400  $\text{cm}^{-1}$  with a resolution of 4  $\text{cm}^{-1}$ . For each sample, 32 scans were collected.

#### 2.2.3 SEM-EDX

SEM-EDX analyses were carried out by using a SNE200M (SEC) microscope equipped with a QUANTAX 100 Advanced BRUKER EDS microanalysis detector. The EDS quantification method is performed by using manufacturer’s standards library and self-calibrating P/B-ZAF standard-based analysis. The images were taken under reduced vacuum conditions on gold coated micro-sample, while the EDS spectra were acquired under reduced vacuum conditions directly on the surface of the micro-sample. The analytical conditions were: 400X magnification, 30 kV, 10 mm working distance.

#### 2.2.4 MA-XRF

MA-XRF analysis was carried out exploiting the scanner designed and developed by the INFN-CHNet (Cultural Heritage Network) collaboration [26] specifically for Cultural Heritage applications [27–29]. The instrument allows to gain elemental spatial maps of a scanned area of the sample. Concisely, the equipment consists of three linear motor stages by Physik Instrumente over which the measuring head is installed. This is composed of a Silicon Drift Detector (Amptek XR100 SDD, 50  $\text{mm}^2$  effective active surface,

**Fig. 1** **A.** S1: albumin photograph representing Trafalgar Square in London (private collection); **B.** S2: a silver bromide photograph, characterized by a surface deterioration (silver mirroring) from a private collection; application of the cleaning treatments onto the analyzed photographs: **C.** Hydrogels on Sample 1, **D.** Calcium chloride on Sample 2



500  $\mu\text{m}$  thickness), an X-ray tube (Moxtek, 40 kV maximum voltage, 0.1 mA maximum anode current) and a telemeter (Keyence IA-100), acting for the continuous control and adjustment of the sample-instrument distance during the scan. In the analysis discussed here, the operating conditions of the X-ray tube were: 38 kV anode voltage, 0.9 mA filament current, Mo anode with an 800  $\mu\text{m}$  diameter collimator. Scanning velocity ranged from 1 to 2 mm/s and the equivalent-pixel size from 200 to 1000  $\mu\text{m}$ .

### 2.2.5 PIXE

PIXE measurements have been carried out at the INFN LABEC laboratory in Florence [30], where is located a 3 MV Tandatron accelerator with an external beamline dedicated to ion beam analysis on cultural heritage samples [31, 32]. A 3 MeV proton beam was used, extracted into atmosphere through a 200 nm thick  $\text{Si}_3\text{N}_4$  membrane. Beam size was defined by a 0.5 mm diameter collimator, placed in vacuum before the extraction window. The photograph was positioned roughly at 1 cm from the beam exit window and measurements lasted 600 s each. Beam current intensity varied between 100 and 200 pA, indirectly measured by means of a rotating chopper [33]. Such measurement conditions resulted in extremely low beam charge densities, guaranteeing the not-deliberately destructive characteristics of these analyses and ensuring no visible effect on the object. The external beam PIXE measurements were performed using simultaneously [21, 34] two X-ray detectors, a 10 mm<sup>2</sup> silicon drift detector (SDD) for light and major elements analysis and a 150 mm<sup>2</sup> SDD, for heavy and trace elements; a He flow was maintained in front of the sample and of the small area PIXE detector in order to reduce the absorption of lower energy X-rays in air.

### 2.2.6 pH measurements

pH measurements were performed on surface paper samples, before and after cleaning procedure, using an Amel Instrument 334-B pH meter with a combined glass electrode Ag/AgCl and a porous PTFE diaphragm (Crison Instruments, Spain); RSD was 1%, calculated on three measurements of the same sample.

## 2.3 Cleaning treatments

### 2.3.1 Materials

The reagents used for the cleaning treatments, poly(vinyl alcohol; fully hydrolyzed) (PVA), calcium chloride and sodium periodate, are acquired from Merck KGaA, Germany. Aqueous solutions were obtained using bi-distilled water (Millipore, Merck, KGaA, Germany).

### 2.3.2 Hydrogels

The application of the cleaning treatments onto the analyzed photographs is shown in Fig. 1. In the case of sample 1 (S1), the cleaning process was performed in selected zones of the photo (Fig. 1C), using two different cleaning gels, called Gel\_L and Gel\_M, characterized by lower (L) and more (M) retentive properties respectively [22, 23]. They are constituted by different molar ratios of PVA and telechelic poly(vinyl alcohol) (called *tel*-PVA). They were prepared according to the protocol reported elsewhere [22, 23]. In the gels (called GEL\_L and GEL\_M), the percentages of PVA and *tel*-PVA are 10 and 5% (w/v) and 10% of PVA and 10% of *tel*-PVA respectively. In detail, *tel*-PVA was prepared by oxidizing the head-to-head PVA sequences using  $\text{NaIO}_4$ , at 2% (mol/mol with respect to the moles of repeating units of PVA) in a solution of PVA at 60 °C under vigorous stirring. After 20 minutes, and cooling the solution at room temperature, the *tel*-PVA solution, was added to an aqueous PVA one (at about 80 °C) to favor the cross-linking of the polymer chains; then pH was adjusted to pH=2 with HCl concentrated solution. To allow the complete gel formation the mixture was left for about 48 hours in the reaction vessel. Finally, the gels were washed against double distilled water for several days until the conductivity of water was about  $1\mu\text{S}$  and no PVA residues were present in the washing water. To perform the cleaning process, a piece of gel was cut to obtain the desired size and applied on the designed zone of the photo. Over them, a PET film was applied, uniformly pressed thus ensuring a close contact between the gel and the sample 1 (S1). Cleaning time was 15 minutes. After cleaning, the gel was removed in only one step.

### 2.3.3 Calcium chloride

In the case of sample 2 (S2), calcium chloride was used as it is to eliminate silver mirroring (Fig. 1D), thus adopting a modification of the method proposed by Mestra J. et al [35]. Several studies reported in literature suggest removing the silver mirroring by washing the sample with water [9, 12, 36]. However, these methods were not applicable to Sample 2, because a washing with water process could have further degraded the photograph, causing swelling of the gelatin. In the treatment proposed by Mestra J. et al [35], the ability of chlorinated hydrocarbons (such as tetrachlorethylene) to not hydrate gelatin is exploited. By cleaning the surface with these solvents, there is no risk to detach the image from the support. At the same time, calcium carbonate, used in the proposed cleaning process, has the advantage of allowing dry alkaline neutralization. Moreover, calcium chloride does not hydrate the surface, rather it is used to dry the area undergoing treatment, removing its moisture. Considering that the treatment proposed by Mestra J. et al [35] could have been a valid tool to remove the silver mirroring from Sample 2, a small amount of calcium chloride was used. Calcium chloride, at room temperature, appears as a white crystalline powder, very hygroscopic, very soluble in water and quite soluble in ethanol, and it was applied and removed onto sample 2 by using a cotton swab (Fig. 2B). The duration of the treatment was approximately 2 minutes.

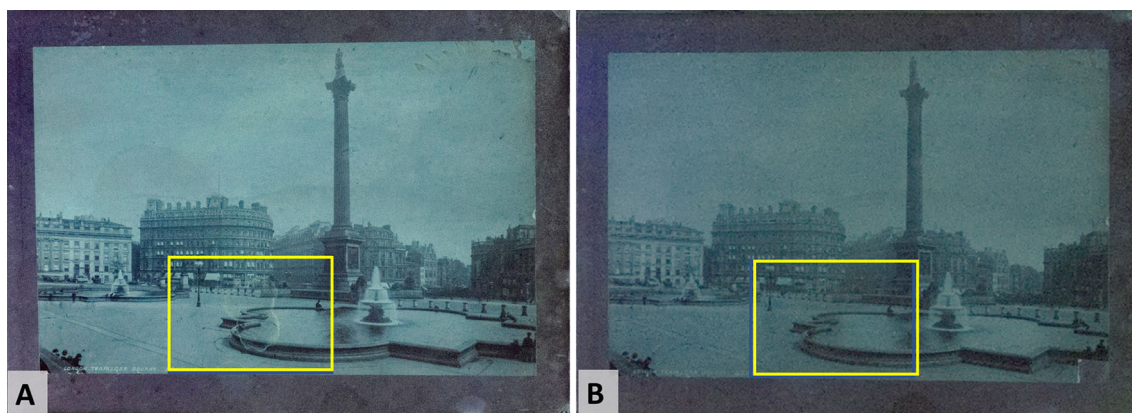


**Fig. 2** A. UV image of Sample 1, the square shows an area characterized by fluorescence spots, B UV image after the cleaning treatments



### 3 Results and discussion

#### 3.1 (S1): Characterization and application of hydrogels to remove albumen degradation products

##### 3.1.1 Pre-treatment characterization

The pre-treatment characterization of S1 by using UV photography showed the presence of two predominant fluorescence signals: indeed, the whole image flows in blue, typical of albumen based tempera [37], while the surface degradation appears as a yellowing of the surface, could be due to the oxidation of aromatic amino acids (tryptophan, tyrosine and phenylalanine) present in albumin and less in gelatin (Fig. 2A). These amino acids are in fact more subject to oxidation [11, 38].

This result was confirmed also by ATR-FTIR analyses which revealed the presence of protein components, identified by Amide I and II bands assigned to the C=O stretching and N-H bending of the peptide bonds, centered at about  $1632\text{ cm}^{-1}$  and  $1526\text{ cm}^{-1}$  respectively (Fig. 3) [1, 39]. The two peaks at the same intensity at about  $1452\text{ cm}^{-1}$  and  $1386\text{ cm}^{-1}$ , related to the stretching mode of lipids, indicate the use of albumin as photograph emulsion. This is confirmed also by a small shoulder of carboxylic groups centered at  $1720\text{ cm}^{-1}$ , together with  $2956$ ,  $2932$  and  $2872\text{ cm}^{-1}$  (relative to CH stretching in aliphatic group) [18, 40]. In addition, the absorption bands at  $3540$  and  $3410\text{ cm}^{-1}$  suggest the presence of gypsum ( $\text{CaSO}_4 \cdot 2(\text{H}_2\text{O})$ ).

The IR spectra of cardboard showed the characteristic band of cellulose (centered at  $1025$  and  $1000\text{ cm}^{-1}$ ) [41]. Regarding the intermediate layer, the one between cardboard and photographic emulsion, the characteristic bands of aluminum silicates (kaolinite ( $\text{Al}_2\text{Si}_2\text{O}_5(\text{OH})_4$ )), at  $3690$ ,  $3620$ ,  $1030$ ,  $1002\text{ cm}^{-1}$  and  $790$ ,  $750\text{ cm}^{-1}$ , as well as gypsum ( $\text{CaSO}_4 \cdot 2(\text{H}_2\text{O})$ ), characterized by bands at about  $3540$ ,  $3410$ ,  $1625$ ,  $1280$ ,  $1150\text{ cm}^{-1}$ , probably used as fillers [42, 43], were detected.

In the spectra acquired (not reported here) in the degraded area (see Fig. 2A) were detected the bands related to albumin, cellulose and gypsum, the same observed for the photographic emulsion [42, 43].

SEM-EDX spectrum was also useful to identify the type of silver halide used for image development (Table 1). The presence of chlorine (Cl) suggested the use of silver chloride in the photographic emulsion. The presence of residual chlorine, not removed by the film development, could represent a potential cause of degradation for the photography due to the possible silver chloride decomposition under light exposure into silver and chloride ions. SEM-EDX also showed the presence of aluminum (Al) and sulfur (S).

Differential PIXE has been essential for the conclusive non-invasive identification of the stratigraphy of the photograph. A selected homogeneous dark, not cleaned, area of Sample 1 was investigated at three different proton energies (2, 3 and 4 MeV in vacuum, corresponding to 1.91, 2.93 and 3.95 MeV on the sample surface respectively, see Fig. 4A). This analysis consists in analyzing the same point of a sample at different proton energies. Since in a layered, or heterogeneous in depth, material the X-ray yields change as a function of the beam energy depending mainly on the elemental distribution and the X-ray absorption in the material itself, the depth profiling of the detected elements can be qualitatively inferred comparing the spectra at different energies. Operatively, for each measurement, first the apparent composition (assuming a homogeneous matrix) was obtained, analyzing the PIXE spectra with the GUPIXWin software package [44]. If the photograph is homogeneous, the same ratios for the composition of the main characteristic elements (Al, Si, K, Fe and Ag) would be expected at different energies [45]. With reference to Fig. 4B, practically the Fe-to-Si, K-to-Si and Al-to-Si composition ratios remained relatively constant at the different energies showing that these elements

**Fig. 3** The FT-IR spectra obtained on three different points of the photographic support: the photographic film (A), the cardboard support (B), the intermediate layer (C) between the cardboard and the photographic film

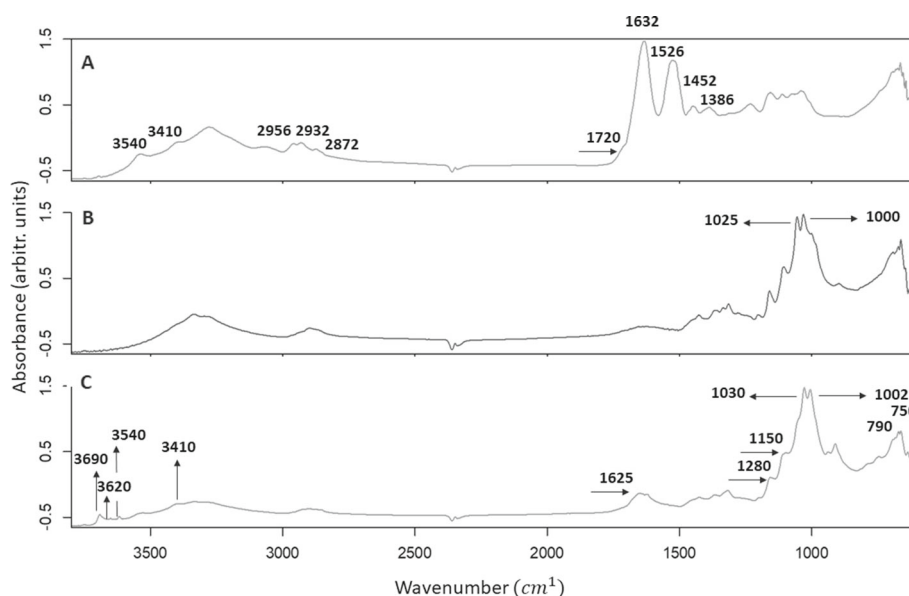


**Table 1** SEM–EDX analysis of S1. Norm. C [wt.%] means the normalized concentration in weight percent of the element with the error in the weight percent concentration at the 1 sigma level

Element	Norm. C. [wt.%]
C	50.32 ± 4.64
O	37.85 ± 4.00
Al	1.24 ± 0.08
Si	1.12 ± 0.07
S	2.21 ± 0.08
Cl	1.56 ± 0.07
Ca	2.17 ± 0.08
Ag	3.52 ± 0.10

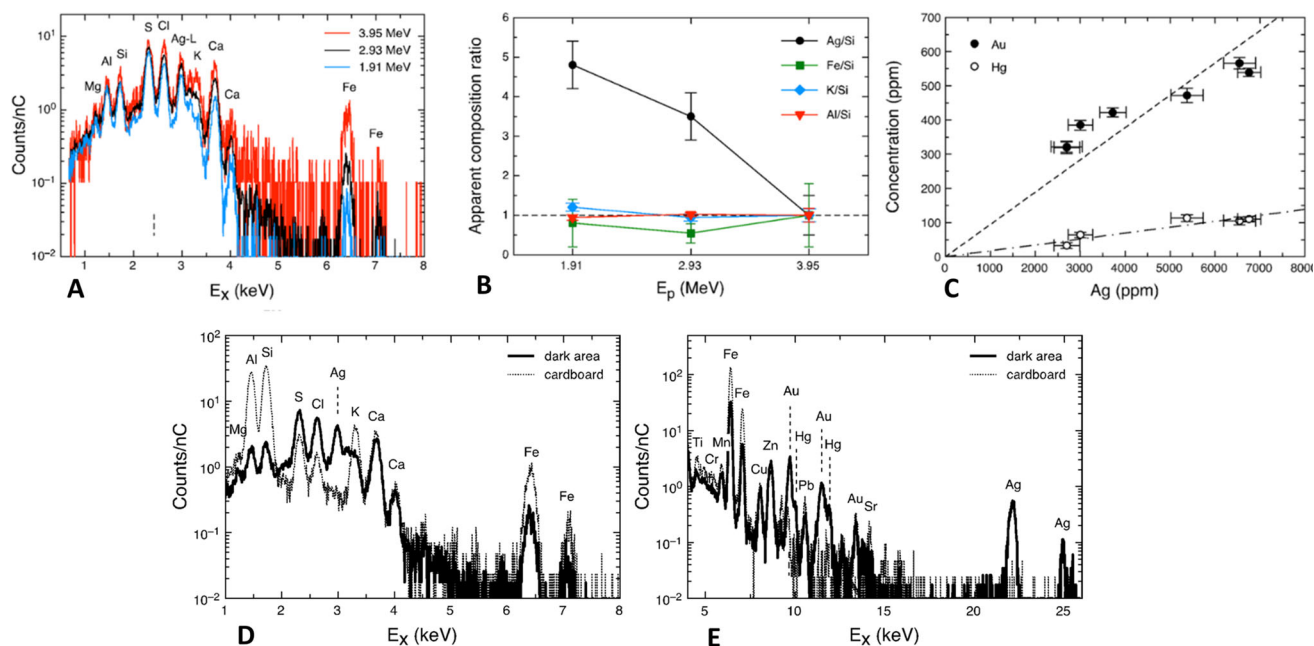


**Fig. 4** **A.** Comparison between PIXE spectra of a dark, not cleaned, area of the photograph at three different energies. The reported beam energies refer to the effective values at the sample surface, after traversing the beam exit window and about 1 cm path in external atmosphere, **B.** Apparent composition ratios of some characteristic elements as a function of the different proton beam energies, **C.** Correlation between the Ag and Au or Hg concentrations in the analyzed spots. Comparison of PIXE spectra obtained analyzing with 3 MeV protons the plain cardboard and a dark, not cleaned, area of the photograph. Spectra on the left refers to the small area SDD for light elements (**D**), while those on the right correspond to the large area SDD for heavy elements (**E**)

**Table 2** pH measurements onto S1 before and after the application of hydrogels

Points	Hydrogels	pH (pre-treatments)	pH (post-treatments)
P1 (back of the photograph)	GEL_L	4.67 ± 0.05	5.18 ± 0.05
P2	GEL_M	4.57 ± 0.05	5.16 ± 0.05
P3	GEL_L	4.64 ± 0.05	5.08 ± 0.05
P4	GEL_M	4.88 ± 0.05	5.12 ± 0.05

could be in the same layer, whereas the Ag-to-Si composition ratio decreased with increasing beam energy evidencing that Ag is present in a more superficial layer than Si (and hence also Al, K and Fe). Two heavy elements, Au and Hg, were found in traces (a few hundreds of ppm) and their concentrations are well correlated with Ag, as shown in Fig. 4C. Au indeed is possibly present in the form of gold thiocyanate or potassium tetrachloroaurate used as chemical sensitizer. Elements as Al and Si are essentially located into the cardboard support, hence comparing the PIXE spectra obtained analyzing with 3 MeV protons the plain cardboard and a dark, not cleaned, area of the S1 photograph, from the attenuation of the X-ray of Al and Si due to the overlaying photograph, it is indeed possible to infer the thickness of the photographic paper. Assuming simply the paper composition as cellulose, C<sub>6</sub>H<sub>10</sub>O<sub>5</sub>, from the different analyzed points of the photograph, it turns out that the thickness of the photographic paper is about 25–40 micrometers.

Moreover, pH measurements were carried out on the back of the photograph (P1) and in different points of the photo (P2, P3 and P4 shown in Fig. 1). The results are presented in Table 2.

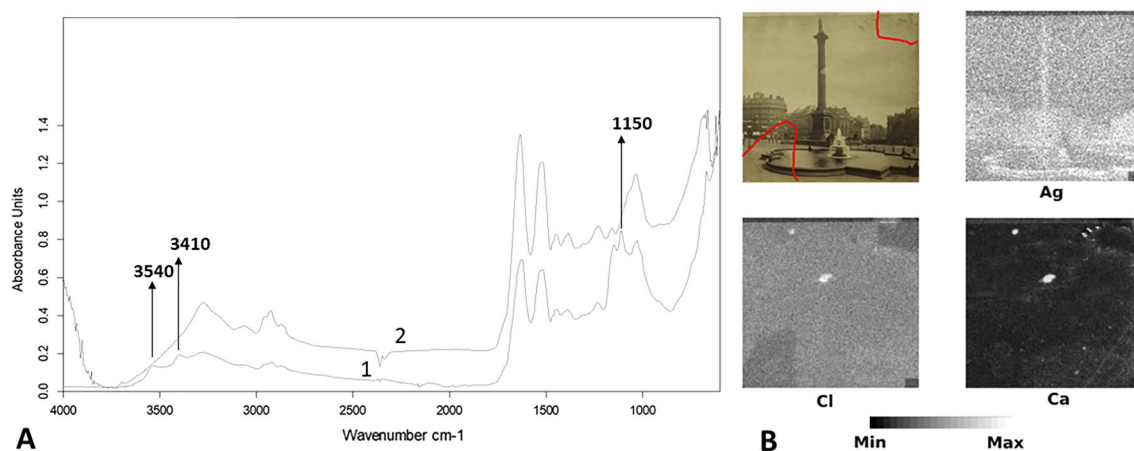


**Fig. 5** **A** FTIR spectra of pre (1) and post (2) cleaning treatments. **B** Details of Sample S1 with relative Ag, Cl, Ca, MA-XRF maps. Cleaning test areas are visible in Cl maps

It should be noted that the pH of a paper in good conservation state is about 7; the very low pH values obtained thus indicate that S1 is strongly oxidized and acid by products are formed. One possibility for slowing down the irreversible degradation process is to use suitable cleaning hydrogels, able to remove dirt and degradation products, improving the pH and the optical quality of the paper support.

### 3.1.2 Application of hydrogels

For this sample, the cleaning treatment adopted was the hydrogel treatment by using two different kinds of gels called GEL\_L, GEL\_M; the first being less retentive than the other. Hydrogels have several advantages: they are easy to synthesize, rigid, transparent, biocompatible and with good retention properties. Desired shaped hydrogels have been applied on the areas that need to be cleaned; these spots have been previously analyzed in order to measure starting pH values. GEL\_L was applied for 15 minutes on point P3, both on the surface of the photo, where there is a patch of dirt (Fig. 1A), and on back of the photograph (P1). GEL\_M, on the other hand, was applied in the same way on points P2 and P4 (Fig. 1A). After the cleaning procedure, GEL\_L did not show any color changes, although it had partially removed the dirty area present on the sample surface. On the contrary, GEL\_M turned yellow, despite removal of the dirt from the photograph was not complete. The yellowing of the gel is probably due to the absorption of cellulose degradation byproducts, due to paper aging, from the cardboard used as a support. It is well known that hydrogels in contact with porous materials can gradually transfer solvent into support and absorb water-soluble materials which move from samples to hydrogels (such as acid molecules due to cellulose degradation), thus carrying out a cleaning action on the paper [22, 23, 46].

### 3.2 Post-treatment characterization

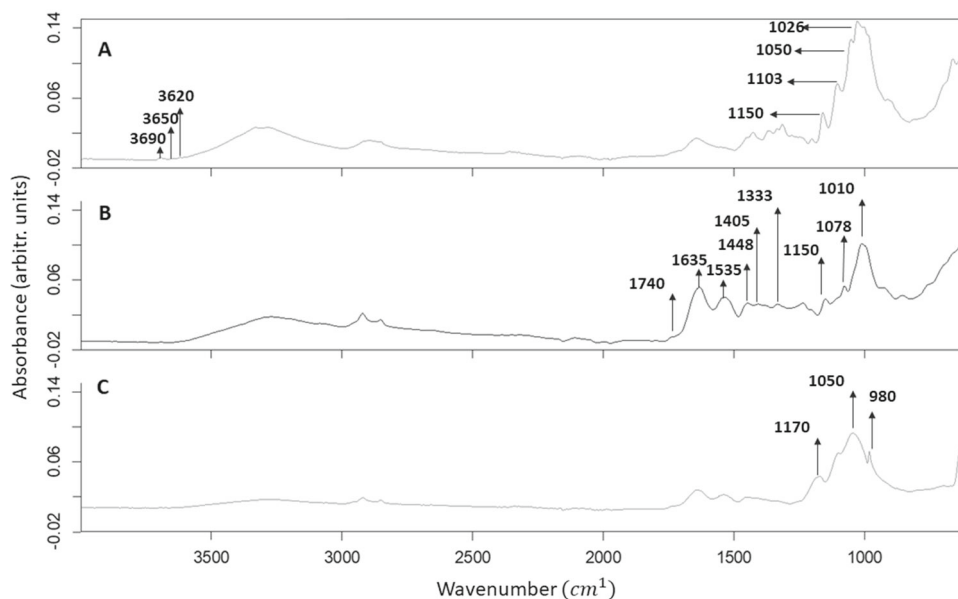
A comparison between the pH values before and after cleaning, reported in Table 2, showed an increase in pH due to treatment, indicating that both the hydrogels used, GEL\_L and GEL\_M, were efficient in removing the acid degradation products present on the sample.

Post-treatment characterization by UV fluorescence images showed the disappearance of the organic material present on the above-discussed area (Fig. 2B), as after the hydrogel treatment no fluorescence was present in the treated area.

After the application of hydrogels, the disappearance of the gypsum bands ( $3540, 3410, 1150 \text{ cm}^{-1}$ ) in the IR spectra was observed, as shown in Fig. 5A. The presence of gypsum on the superficial layer could be due to a rise of the gypsum from the underlying layer. The fact that after cleaning with hydrogel it is no longer visible could mean that it has been mechanically removed or has been solubilized in the hydrogel.

The XRF maps of Sample S1, shown in Fig. 5, show the Ag distribution that corresponds to the darker areas of the image (impressed areas). The effectiveness of cleaning methods is confirmed by observing the chlorine (Cl) map: the element appears partially removed in the treated areas.

**Fig. 6** FT-IR spectra of cardboard support (A), silver mirroring film (B), white layer (C)



### 3.3 Sample 2 (S2): Silver photograph (Gelatin silver print DOP) a stratigraphic characterization and cleaning treatment dissertation

#### 3.3.1 Pre-treatments characterization

Thanks to a deterioration present on the upper left side of the sample 2 (S2), it was possible to analyze, by means of FT-IR, three different layers: the support, a white substance and the surface affected by silver mirroring effect (Fig. 6).

The FT-IR spectrum of the paper support of S2 showed the main absorption bands of cellulose (1150, 1103, 1050, 1026, 910  $\text{cm}^{-1}$ ) and the absorption bands at about 3690, 3650 and 3620  $\text{cm}^{-1}$ , that characterize aluminum silicates (kaolin), often used as fillers in paper supports as already explained [42].

FT-IR detects starch (1150, 1078, 1010  $\text{cm}^{-1}$ ) and gelatin (1635, 1535, 1448, 1405 e 1333  $\text{cm}^{-1}$ ) [47, 48] that are the constituents of the emulsion, and a band at about 1740  $\text{cm}^{-1}$ , probably related to the presence of organic acids. The white substance, superimposed on the paper, was identified as baryte (1170, 1050, 980  $\text{cm}^{-1}$ ) [49].

On the basis of these results, the Sample 2 is a gelatin silver photograph. Further, the presence of a mirror effect confirms the manufacturing technique.

Once the stratigraphy of the photograph analyzed has been defined, our attention was focused on the areas where silver mirroring was present and on its removal.

IR Reflectography (IRR) has indicated that, below the silver mirroring layer of S2, some parts of the image were still intact (Fig. 6B). Indeed, the IRR image as allowed to recover features of the photo no more visible at naked eye, as for example, the branches of the tree, the gentleman's jacket and tree trunks, confirming the existence of a still well-defined image below the patina layer, except for the bottom part that is completely degraded (Fig. 7).

The SEM-EDX analysis (Table 3) showed the presence of Si and Al, attributed to kaolin, used as a filler in the paper support, while chlorine (Cl) suggests that this is the halogen used to perform the photographic emulsion, as the sample S. Sulphur and barium are related to baryte layer.

#### 3.3.2 Application of calcium Chloride

As previously discussed, calcium chloride was applied and removed on the photo with the help of a cotton swab, the application time was around 2 minutes.

#### 3.3.3 Post-treatments characterization

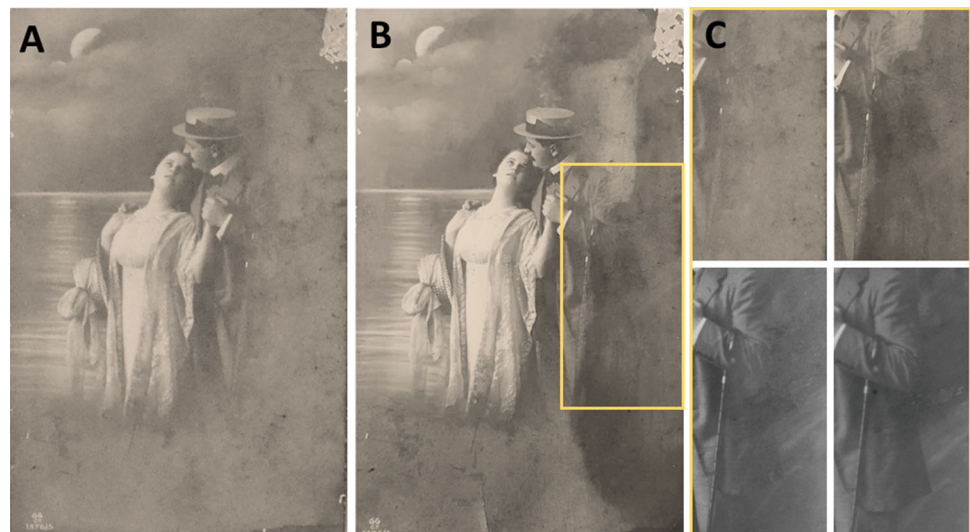
The effectiveness of the treatment is directly observable from the image shown in Fig 8. Indeed, silver mirroring affected areas were partially removed and some details have come to light (Fig. 8C). The IRR image captured after the treatment showed that other details are present below the treated surface.

SEM image showed that the surface appears more compact and no longer encrusted with respect to the silver mirroring one, however a deposit of calcium chloride occurs by means the SEM – EDX maps of Ca and Cl (Fig. 9).



**Fig. 7** Photo **A** and IRR image **B** of S2**Table 3** SEM–EDX analysis of S2. Norm. C [wt.%] means the normalized concentration in weight percent of the element with the error in the weight percent concentration at the 1 sigma level

Element	Norm. C. [wt.%]
C	26.51 ± 4.42
O	11.02 ± 2.36
Al	0.64 ± 0.09
Si	0.77 ± 0.08
S	5.81 ± 0.20
Cl	9.39 ± 0.26
K	2.59 ± 0.11
Ca	2.97 ± 0.12
Ag	15.30 ± 0.38
Ba	24.98 ± 0.50

**Fig. 8** Photo (A), IRR image (B) of S2 and (C) magnification of Photo and IRR detail that shows the partially removal of silver mirroring

These results are consistent with those obtained by MA-XRF mapping, shown in Fig. 10, where in the Ca and Cl maps the cleaning test areas are clearly visible. The higher X-ray counts of these two elements in the lower right corner of the photograph may suggest an incomplete removal of the cleaning treatment.

**Fig. 9** Secondary electron (SE) image pre **A** and post **B** treatment of S2; Back scattered electron (BSE) image after the treatment **C** and Ca and Cl maps (**D** and **E**)

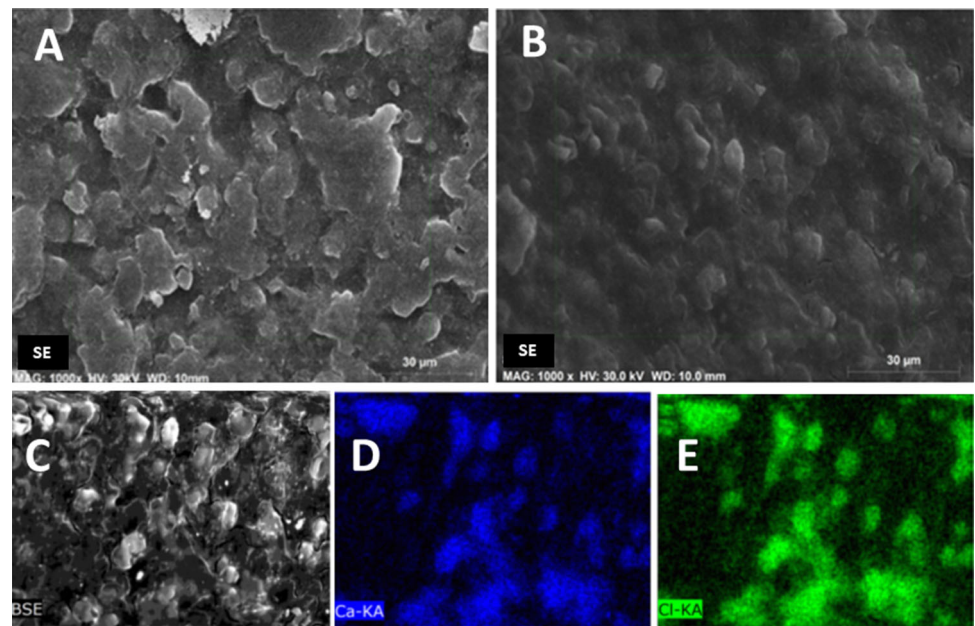
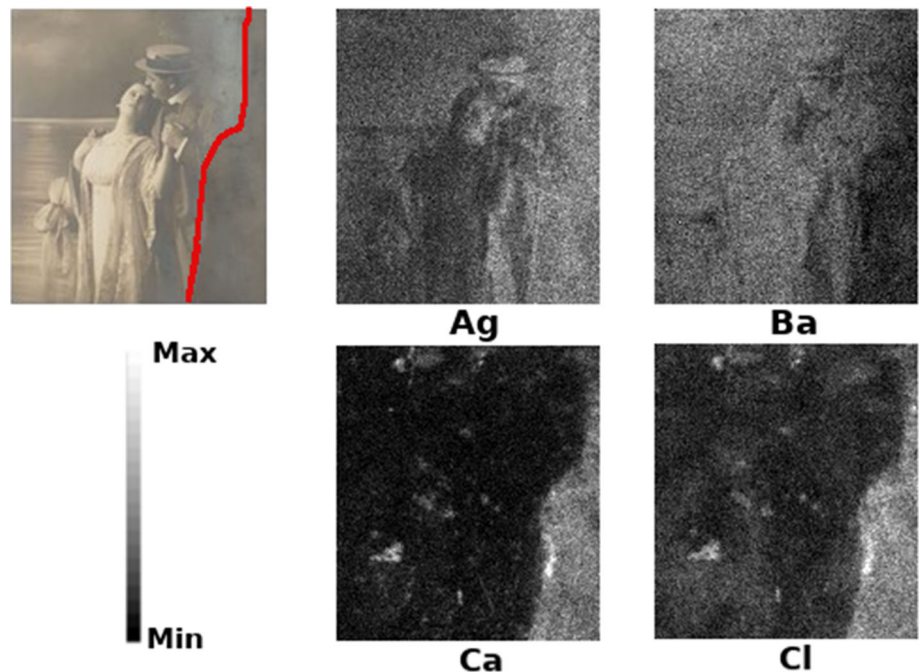


**Fig. 10** A Detail of Sample S2 with relative Ag, Ba, Ca, Cl MA-XRF maps. Cleaning test areas are visible in Cl and Ca maps



#### 4 Conclusions

This work is focused on the evaluation of two cleaning methods of degradation products onto ancient photographs. In particular, two types of photographs were analyzed, an albumen print and a silver gelatin one, by using a multi-analytical approach. The imaging techniques have proved useful for making an initial diagnosis of the conservation state of the analyzed samples. The FT-IR analysis has proven to be a powerful tool for identifying binders and supports, allowing to discriminate between gelatin and albumin as a material used as binder, and providing information about the composition of the paper support and the fillers used during the manufacturing process. Elemental analyses (SEM-EDX and mapping XRF) were used to identify the elemental composition of the samples, and to map their distribution onto the photography surface. Finally, differential PIXE has been essential for the conclusive non-invasive identification of the stratigraphy of the sample 1. Matching the data obtained from this multi-analytical approach it was possible to choose a dedicated cleaning treatment for each analyzed sample. Therefore, in the case of sample 1, wet treatment using opportune hydrogels was effective to improve the conservation state of the photographic surface. Instead, sample 2 was treated with calcium chloride, exploiting its dehydrating power, in order to remove the silver mirroring. After the cleaning treatment, a second

characterization was carried out, using the same analytical approach previously described, to verify the effectiveness of the cleaning methods used.

About Sample 1, the obtained results showed an increase in pH values suggesting the efficacy of the selected treatment. The effectiveness of cleaning treatments is visible also in the XRF map of Sample 1, where the chlorines (Cl) present on the surface layer result to be partially removed. A comparison between the pH values before and after cleaning, reported in Table 2, showed an increase in pH, indicating that both the used hydrogels, GEL\_L and GEL\_M, were efficient in removing the acid degradation products present on the sample.

About Sample 2, calcium chloride was effective to remove the silver mirroring effect, recovering the photographic image. However, the elemental analysis (SEM-EDX and MA-XRF) showed the presence of chlorine and calcium, suggesting that the calcium chloride remains on the surface. Thus, this process must be further improved.

The results discussed in this work represent a preliminary study of different cleaning treatments applied on two case study. However, in order to prove the effectiveness of the proposed method, other typologies of photography will be treated and analyzed.

**Acknowledgements** Parts of this work were carried out during the bachelor degree of A.D. "Analisi spettroscopiche su materiale fotografico: Caratterizzazione di materiale fotografico risalente al secolo scorso e messa a punto di metodi idonei di pulitura". Thanks to C.G. for the possibility to analyze the Sample 2 from her private collection. Thanks to A.R., A.G., M.P. of DAFNE-Light Synchrotron Radiation Facility of INFN-Laboratori Nazionali di Frascati for their technical support to the experiments. Thanks to prof. G.P. and Dr.F.D. for suggestions in hydrogels preparation. All the INFN activities related to Cultural Heritage were realized in the field of INFN-Cultural Heritage Network (CHNet).

**Author contributions** M.R., L.P., C.R., M.C.G. and C.M. contributed to conceptualization; M.R., L.P., C.R., M.C.G., C.M. and L.S. contributed to methodology; A.D., M.R., L.P., C.R., A.M., L.S., M.C., L.C. and G.V. performed investigation; M.C.G., F.T., M. A. and C.M. provided resources; M.R., L.P., C.R., A.M., L.S., M.C., L.C., A.D. and C.M. contributed to data curation and data analyses; M.R. performed writing—original draft preparation; M.R., L.P., C.R., A.M., C.M., M.C., L.C. and M.C.G. performed writing—review and editing; M.R., L.P., M.C.G., C.G., M. A. and C.M. performed review and supervision. All authors have read and agreed to the published version of the manuscript.

**Funding** No funding.

**Data Availability Statement** All data discussed in this work are available by sending an email to the corresponding author.

## Declarations

**Conflict of interest** The authors declare no conflict of interest.

## References

1. A. Vila, S. Centeno, *Microchem. J.* (2013). <https://doi.org/10.1016/j.microc.2012.07.016>
2. E. Grieten, J. Caen, D. Schryvers, *Microsc. Microanal.* (2014). <https://doi.org/10.1017/S1431927614012860>
3. B. Cattaneo, D. Chelazzi, R. Giorgi, R., T. Serena, C. Merlo, & P. Baglioni, *J. Cult. Herit.* **9** (2008). <https://doi.org/10.1016/j.culher.2008.01.004>
4. A. Nieto-Villena, J.R. Martínez, J.M. Flores-Camacho, A. Lastras-Martínez, J.A. de la Cruz-Mendoza, G. Ortega-Zarzosa, J.C. Valcárcel-Andrés, A. Solbes-García, *Stud. Conserv.* (2018). <https://doi.org/10.1080/00393630.2018.1476962>
5. L. Costa, M. Nunes, S. Costa, M. Trindade, C. Miguel, T. Ferreira, *Microsc. Microanal.* (2019). <https://doi.org/10.1017/S1431927618000429>
6. J.P. McElhone, *Top. Photogr. Preserv.* **5**, (1993)
7. A. Puškárová, M. Bučková, B. Habalová, L. Kraková, A. Maková, D. Pangallo, *Sci. Rep.* **6**, 1–14 (2016). <https://doi.org/10.1038/srep20810>
8. M.C. Sclocchi, E. Damiano, D. Matè, P. Colaizzi, F. Pinzari, *Int. Biodeterior. Biodegrad.* (2013). <https://doi.org/10.1016/j.ibiod.2012.04.021>
9. G. Marucci, A. Monno, I.D. van der Werf, *Microchem. J.* (2014). <https://doi.org/10.1016/j.microc.2014.07.001>
10. G. Di Pietro, in *Proceedings of Metal 2004 National Museum of Australia Canberra ACT* (2004)
11. O. Mantovani, G. Impagliazzo, D. Ruggiero, M.T. Tanasi, L. Botti, L. Residori, & M.C. Sclocchi, *Chimica e biologia applicate alla conservazione degli archivi.* (PUBBLICAZIONI DEGLI ARCHIVI DI STATO SAGGI 742002).
12. B. Lavédrine, J-P. Gandolfo, M. Frizot, S. Monod, *Photographs of the Past: Process and Preservation*, **352**. (Getty Conservation Institute 2009). ISBN 978-0-89236-957-7
13. D.L. Mac Adam, *J. Photogr. Sci.* **14**(5), (1966). <https://doi.org/10.1080/00223638.1966.1173736>
14. A. Aldrovandi, D. Bertani, M. Cetica, M. Matteini, A. Moles, P. Poggi, P. Tiano, *Stud. Conserv.* (1988). <https://doi.org/10.1179/sic.1988.33.3.154>
15. D. Comelli, G. Valentini, A. Nevin, A. Farina, L. Toniolo, R. Cubeddu, *Rev. Sci. Instrum.* (2008). <https://doi.org/10.1063/1.2969257>
16. L. Pronti, M. Romani, O. Tarquini, G. Verona-Rinati, F. Petrucci, M. Colapietro, A. Pifferi, M. Marinelli, M. Cestelli-Guidi, *Eur. Phys. J. Plus.* (2020). <https://doi.org/10.1140/epjp/s13360-020-00607-1>
17. D. Stulik, V. Dorge, H. Khanjian, N. Khandekar, A.D. Tagle, D. Miller, R. Wolbers, J. Carlson, . *Progetto Restauro, Trimestrale per la tutela dei Beni Culturali.* (2002) <http://www.openbibart.fr/item/display/10068/846506>
18. C. Ricci, S. Bloxham, S.G. Kazarian, *J. Cult. Herit.* (2007). <https://doi.org/10.1016/j.culher.2007.07.002>
19. S. Casoli, S. Fornaciari, *Microchem. J.* (2014). <https://doi.org/10.1016/j.microc.2014.04.003>
20. L. Pronti, M. Romani, G. Viviani, C. Stani, P. Gioia, M.C. Guidi, *Rend. Lincei* **31**, 485–493 (2020). <https://doi.org/10.1007/s12210-020-00888-9>

21. M. Vadrucchi, A. Mazzinghi, A. Gorghinian, L. Picardi, C. Ronsivalle, C. Ruberto, M. Chiari, Appl. Radiat. Isot. (2019). <https://doi.org/10.1016/j.apradiso.2018.10.016>
22. C. Mazzuca, L. Severini, M. Missori, M. Tumiati, F. Domenici, L. Micheli, M. Titubante, M. Bragaglia, F. Nanni, G. Paradossi, A. Palleschi, Microchem. J. **155**, 104716 (2020). <https://doi.org/10.1016/j.microc.2020.104716>
23. C. Mazzuca, L. Severini, F. Domenici, Y. Toumia, F. Mazzotta, L. Micheli, M. Titubante, B. Di Napoli, G. Paradossi, A. Palleschi, Colloids Surfaces B Biointerfaces **188**, 110777 (2020). <https://doi.org/10.1016/j.colsurfb.2020.110777>
24. T. Luzeckyj, I. Bruckle, Top. Photogr. Preserv. **8**, (1999). Published by the Photographic Materials Group (PMG) of the American Institute for Conservation of Historic & Artistic Works (AIC)
25. G. Ntasi, D.P. Kirbyb, I. Stanzione, A. Carpentieria, P. Somma, P. Cicatiello, G. Marinao, P. Giardina, L. Birolo, G. Ntasi, J. Proteomics **231**, 104039 (2021). <https://doi.org/10.1016/j.jprot.2020.104039>
26. F. Taccetti, L. Castelli, C. Czelusniak, N. Gelli, A. Mazzinghi, L. Palla, C. Ruberto, C. Corsori, A. Lo Giudice, A. Re, D. Zafirooulos, F. Arneodo, V. Conicella, A. Di Giovanni, R. Torres, F. Castella, N. Mastrangelo, D. Gallegos, M. Tascon, F. Marte, L. Giuntini, Lincei. Scienze Fis. Nat. **1**, 3 (2019). <https://doi.org/10.1007/s12210-018-0756-x>
27. A. Mazzinghi, C. Ruberto, L. Castelli, C. Czelusniak, L. Giuntini, P.A. Mandò, F. Taccetti, Appl. Sci. (2021). <https://doi.org/10.3390/app11136151>
28. A. Mazzinghi, C. Ruberto, L. Castelli, P. Ricciardi, C. Czelusniak, L. Giuntini, P.A. Mandò, M. Manetti, L. Palla, F. Taccetti, X-ray Spectrom. **50**, 272–278 (2021). <https://doi.org/10.1002/xrs.3181>
29. L. Sottili, L. Guidorzi, A. Mazzinghi, C. Ruberto, L. Castelli, C. Czelusniak, L. Giuntini, M. Massi, F. Taccetti, M. Nervo, S. De Blasi, R. Torres, F. Arneodo, A. Re, A. Lo Giudice, Appl. Sci. (2021). <https://doi.org/10.3390/app11031197>
30. M. Chiari, S. Barone, A. Bombini, G. Calzolari, L. Carraresi, L. Castelli, C. Czelusniak, M.E. Fedi, N. Gelli, F. Giambi, F. Giardi, L. Giuntini, S. Lagomarsino, L. Liccioli, F. Lucarelli, M. Manetti, M. Massi, A. Mazzinghi, S. Nava, P. Ottanelli, S. Sciortino, C. Ruberto, L. Sodi, F. Taccetti, P.A. Mandò, Eur. Phys. J. Plus **136**, 472 (2021). <https://doi.org/10.1140/epjp/s13360-021-01411-1>
31. L. Giuntini, L. Castelli, M. Massi, M. Fedi, C. Czelusniak, N. Gelli, F. Taccetti, Appl. Sci. (2021). <https://doi.org/10.3390/app11083462>
32. M. Vadrucchi, A. Mazzinghi, B. Sorrentino, S. Falzone, C. Gioia, P. Gioia, E.M. Loreti, M.C. Vadrucchi, X-Ray Spectrom. **49**, 668–678 (2020). <https://doi.org/10.1002/xrs.3178>
33. M. Chiari, A. Migliori, P.A. Mandò, Nucl. Instrum. Methods Phys. Res. Sect. B: Beam Interact. Mater. At. (2002). [https://doi.org/10.1016/S0168-583X\(01\)01067-9](https://doi.org/10.1016/S0168-583X(01)01067-9)
34. C. Jeynes, M.J. Bailey, N.J. Bright, M.E. Christopher, G.W. Grime, B.N. Jones, V.V. Palitsin, R.P. Webb, Nucl. Instrum. Methods Phys. Res. Sect. B: Beam Interact. Mater. At. **271**, 107–118 (2012). <https://doi.org/10.1016/j.nimb.2011.09.020>
35. J. Mestre, J. M<sup>a</sup> Vergés, El mirall de plata en les fotografies: importància, mecanisme d'aparició i nou procediment d'eliminació, (Únicum (17) 2018. Ed. ESCRBCC (Escola Superior de Conservació i Restauració de Béns Culturals de Catalunya). ISSN: 1579-3613
36. B. Lavédrine, J. P. Gandolfo, S. Monod, A guide to the preventive conservation of photograph collections. (Getty Publications 2003). ISBN 0-89236-701-6
37. International Preservation News, A Newsletter of the IFLA Core Activity on Preservation and Conservation **55** (2011). ISSN 0809-4690
38. S. Guedes, R. Vitorino, R. Domingues, F. Amado, P. Domingues, Rapid Commun. Mass Spectrom. (2009). <https://doi.org/10.1002/rcm.4149>
39. E. Ghiocel Ioanid, A. Ioanida, D.E. Rusub, C.-M. Popescua, I. Stoica, J. Cult. Herit. (2011). <https://doi.org/10.1016/j.culher.2011.04.002>
40. C. Duce, L. Ghezzi, M. Onor, I. Bonaduce, M.P. Colombini, M.R. Tine, E. Bramanti, Anal. Bioanal. Chem. **402**, 2183–2193 (2012). <https://doi.org/10.1007/s00216-011-5684-x>
41. P. Garside, P. Wyeth, Restaurator **25** (2004). <https://doi.org/10.1515/REST.2004.249>
42. M. Sbroscia, M. Cestelli-Guidi, F. Colao, S. Falzone, C. Gioia, P. Gioia, C. Marconi, D. Mirabile Gattia, E.M. Loreti, M. Marinelli, M. Missori, F. Persia, L. Pronti, M. Romani, A. Sodo, G. Verona-Rinati, M.A. Ricci, R. Fantoni, Microchem. J (2020). <https://doi.org/10.1016/j.microc.2019.104450>
43. K. Howe, K.P. Ishida, M.M. Clark, M.M. Clark, Desalination (2002). [https://doi.org/10.1016/S0011-9164\(02\)00545-3](https://doi.org/10.1016/S0011-9164(02)00545-3)
44. J.A. Maxwell, J.L. Campbell, W.J. Teesdale, Nucl. Instrum. Methods Phys. Res. Sect. B: Beam Interact. Mater. At. (2010). [https://doi.org/10.1016/0168-583X\(89\)90042-6](https://doi.org/10.1016/0168-583X(89)90042-6)
45. O. Enguita, A. Climent-Font, G. García, I. Montero, M.E. Fedi, M. Chiari, F. Lucarelli, Nucl. Instrum. Method. Phys. Res. Sect. B: Beam Interact. Mater. At. (2002). [https://doi.org/10.1016/S0168-583X\(01\)01081-3](https://doi.org/10.1016/S0168-583X(01)01081-3)
46. C. Mazzuca, G. Poggi, N. Bonelli, L. Micheli, P. Baglioni, A. Palleschi, J. Colloid Interface Sci. **502**, 153–164 (2017). <https://doi.org/10.1016/j.jcis.2017.04.088>
47. M. Prochoń, A. Marzec, B. Szadkowski, Materials (Basel). **12**, 1684 (2019). <https://doi.org/10.3390/ma12101684>
48. S. Taokaew, S. Seetabhwang, P. Siripong, M. Phisalaphong, Materials (Basel). **6**, 782–794 (2013). <https://doi.org/10.3390/ma6030782>
49. F. Jones, CrystEngComm **14**, 8374–8381 (2012)